
Spotlight Attention: Robust Object-Centric Learning With a Spatial Locality Prior

Ayush Chakravarthy
Mila, Université de Montréal
ayush.k.chakravarthy@gmail.com

Trang Nguyen
Mila, Université de Montréal

Anirudh Goyal
Google DeepMind

Yoshua Bengio
Mila, Université de Montréal

Michael C. Mozer
Google Research, Brain Team

Abstract

The aim of object-centric vision is to construct an explicit representation of the objects in a scene. This representation is obtained via a set of interchangeable modules called *slots* or *object files* that compete for local patches of an image. The competition has a weak inductive bias to preserve spatial continuity; consequently, one slot may claim patches scattered diffusely throughout the image. In contrast, the inductive bias of human vision is strong, to the degree that attention has classically been described with a spotlight metaphor. We incorporate a spatial-locality prior into state-of-the-art object-centric vision models and obtain significant improvements in segmenting objects in both synthetic and real-world datasets. Similar to human visual attention, the combination of image content and spatial constraints yield robust unsupervised object-centric learning, including less sensitivity to model hyperparameters.

1 Introduction

Learning about objects and their interactions is a cornerstone of human cognition [Spelke and Kinzler, 2007]. Understanding the nature of objects and their properties is necessary to achieve symbol-like mental representations [Whitehead, 1928] and systematicity of reasoning [Fodor and Pylyshyn, 1988]. Although language has a natural tokenization that supports systematicity [Chakravarthy et al., 2022], progress in visual reasoning in Artificial Intelligence hinges on tokenizing visual input. Visual tokenization corresponds to the problem of *object-centric representation learning*—learning to partition images into a set of discrete slots in an unsupervised manner. The desiderata for these slots are that they induce a bijection with the objects in an image and are interchangeable.

With no or limited supervision, object-centric representation learning is very difficult [Greff et al., 2020] and requires appropriate forms of inductive bias [Schölkopf et al., 2021, Ke et al., 2021, Goyal and Bengio, 2022]. The biases explored for building models with object-centric representation have been based on instance based segmentation [Greff et al., 2017, 2019a, Locatello et al., 2020], sequential object extraction [Gregor et al., 2015, Burgess et al., 2019, Engelcke et al., 2021, Goyal et al., 2021a], invariance [Crawford and Pineau, 2019, Lin et al., 2020, Jiang et al., 2020, Biza et al., 2023], type-token distinction [Bao et al., 2022, 2023, Goyal et al., 2020] and the sparsity of interactions among different slots [Goyal et al., 2021b,c].

However, none these methods leverage a bias that is considered fundamental to visual attention in the psychological literature: the preference for spatial continuity of an attended region. Traditionally, attention was considered to be a *spotlight* on a region of interest in the image [Posner, 1980]. The spotlight metaphor was extended to be a zoom lens [LaBerge, 1983], allowing for large or small

regions, but nonetheless the regions needed to be convex. The metaphor was further extended to allow the selected region to blanket around a shape [Mozer, 1988]. In the psychological literature, even the notion of *object-based attention* [Duncan, 1984] is spatial in nature [Vecera and Farah, 1994], although it allows noncontiguous features of an object to be selected together e.g., if two ends of an occluded object are visible [Zemel et al., 2002].

Although current techniques in object-centric representation learning make available a positional encoding to guide the mapping between image patches and slots, the slot extraction process itself has no explicit pressure to choose patches in a spatially contiguous manner. Consequently, one slot may claim patches scattered diffusely throughout the image. In this paper, we introduce an inductive bias in the form of a *spatial locality prior (SLP)* that encourages slots to select spatially contiguous patches in the input image.

Summary. We present an algorithm that can be incorporated into models for object-centric representation learning that biases slot assignments based on spatial locality. We show consistent improvements in the quality of object representations for three object-centric architectures, eight distinct data sets, both synthetic and natural, and multiple different performance measures that have been used in the literature. We show that the SLP also makes the baseline models more robust to hyperparameter selection and supports robust out-of-distribution generalization.

2 Background

Unsupervised Object-Centric Learning. Our work falls into the line of research in machine vision known as unsupervised object-centric representation learning [Eslami et al., 2016, Greff et al., 2017, 2019a, Burgess et al., 2019, Goyal et al., 2020, Lin et al., 2020, Locatello et al., 2020, Engelcke et al., 2021, Singh et al., 2022a, Jia et al., 2023]. Broadly, this work has the objective of mapping image elements to a low-dimensional set of objects, or *slots*, where the goal is for grouped image elements to be semantically similar. As ‘semantic similarity’ is an ambiguous objective, several additional sources of information have been explored including video sequences [Jiang et al., 2020, Weis et al., 2021, Singh et al., 2022b, Traub et al., 2023] and optical flow [Kipf et al., 2022, Elsayed et al., 2022, Bao et al., 2022, 2023]. However, as pointed out by Yang and Yang [2022], such methods suffer from problems in scaling to large real-world datasets. Toward alleviating this problem, recent work has moved from CNNs to Transformer-based models which have greater expressivity [Singh et al., 2022a, Seitzer et al., 2023]. Nonetheless, the basic mechanism of slot assignment in Slot Attention [Locatello et al., 2020] and its variants [Chang et al., 2022, Jia et al., 2023] has proven a critical building block to unsupervised object-centric learning.

Spatially-biased OCL. The key novelty of our work is a spatial-proximity-based mechanism that modulates the slot-pixel assignment. One might argue that because current methods for object centric representation learning includes explicit positional encodings in its input [Locatello et al., 2020, Goyal et al., 2020, 2021b], the existing methods have sufficient information to discover the principle of spatial coherence. However, the results we present clearly indicate otherwise, or at least that spatial constraints have yet to be fully exploited. Other work has incorporated spatial information into models, such as using shape priors for weak supervision [Elich et al., 2020], spatial position as a means to bootstrap learning [Kim et al., 2023], and incorporating spatial symmetries [Biza et al., 2023]. Furthermore, in the context of video, SaVi [Kipf et al., 2022] and SaVi++ [Elsayed et al., 2022] use ground-truth spatial information such as center of mass and bounding boxes extracted from the first frame of the video. However, our method is the first to use spatial constraints to steer the slot-pixel assignment with no supervision.

3 Method

3.1 Augmenting Key-Query Match with Spatial Bias

The input image is first pre-processed by an *image encoder*. This processing preserves the image topography, yielding an embedding at each image patch p , which corresponds to an (x, y) position in a coarse grid over the image. (The embedding is intended to encode high-level visual features, and thus the grid of patches is coarser than the input dimensions in pixels.) The embedding at each patch p is mapped to a key, κ_p , which is matched to a query from each slot k , denoted q_k . The evidence

supporting a key-query match is

$$\gamma_{kp} = \frac{\mathbf{q}_k^T \boldsymbol{\kappa}_p}{\sqrt{d}},$$

where d is the dimensionality of the query and key vectors.

In various different methods of object centric representation learning [Goyal et al., 2020, Locatello et al., 2020, Goyal et al., 2021b], slots compete for each grid position via a softmax renormalization of the match scores γ_{kp} . Here, we introduce a *Spatial Locality Prior* to modulate the competition among slots. This prior takes the form of an additive term, α_{kp} , in the softmax:

$$s_{kp} = \text{softmax}_k(\gamma_{kp} + \alpha_{kp}),$$

where s_{kp} is the affinity between position p and slot k , and softmax_k denotes the k 'th element of the softmax vector. We use $\mathbf{s}_k \equiv \{s_k\}$ to denote the distribution of activation (or attention) over positions for a given slot k . The $\boldsymbol{\alpha}$ matrix is used to bias this distribution by spatial locality.

3.2 Encouraging Spatial Locality

Conditioned on an input, the $\boldsymbol{\alpha}$ matrix is determined by a constraint satisfaction process (CSP) that encourages a roughly spotlight-like distribution of activation over positions in \mathbf{s}_k for each slot k . Additionally, the CSP discourages overlap in the spotlights of any pair of slots. The CSP converges on $\boldsymbol{\alpha}$ by iterative gradient-descent steps in a loss that penalizes spotlights that are non-compact and overlapping.

The spotlight associated with each slot k is characterized by its center, \mathbf{m}_k , and isotropic spread, v_k , defined to be the central tendency and variance of \mathbf{s}_k :

$$\mathbf{m}_k = \frac{\sum_p s_{kp} \mathbf{p}}{\sum_p s_{kp}} \quad \text{and} \quad v_k = \frac{\sum_p s_{kp} |\mathbf{p} - \mathbf{m}_k|^2}{\sum_p s_{kp}} \quad (1)$$

Note that while $\sum_k s_{kp} = 1$ due to the softmax, the sum over positions is not normalized.

The CSP's loss consists of two terms. First, a penalty is imposed to the degree that each pair of slots fail to have spatially distinct attentional profiles, as characterized by a distance measure summed over slot pairs:

$$\mathcal{L}_{\text{distinct}} = \sum_{k, k' > k} \exp\left(-\frac{|\mathbf{m}_k - \mathbf{m}_{k'}|^2}{v_k + v_{k'}}\right) \quad (2)$$

This loss is designed to push apart the slot means (the numerator term) relative to the intra-slot variance (the denominator term). Second, to prevent degenerate solutions in which attention collapses to a point, we impose a penalty on the Froebenius norm of $\boldsymbol{\alpha}$:

$$\mathcal{L}_{\text{norm}} = \sum_{k,p} \alpha_{kp}^2 \quad (3)$$

The overall loss $\mathcal{L} = \mathcal{L}_{\text{distinct}} + \lambda \mathcal{L}_{\text{norm}}$ is minimized with respect to $\boldsymbol{\alpha}$ from an initial state $\boldsymbol{\alpha}^0$, which we discuss next.

3.3 Learning Initial State Through Bilevel Optimization

To break symmetry, it is vital to learn an initial state $\boldsymbol{\alpha}^0$ which partitions the image by dispersing initial slot means across the image. We take inspiration from Jia et al. [2023] and perform meta-learning to determine $\boldsymbol{\alpha}^0$. On each training trial, after j steps of the CSP optimization, we obtain an approximately optimal attentional bias, let's call it $\boldsymbol{\alpha}^*$. We detach $\boldsymbol{\alpha}^*$ and optimize for $\boldsymbol{\alpha}^0$ on the last CSP step. We use the straight-through estimator [Bengio et al., 2013, van den Oord et al., 2017] to additionally propagate gradients into $\boldsymbol{\alpha}^0$. Through this design, we are able to learn generalized dataset-wide statistics about $\mathbb{E}[\mathbf{m}_k]$ and $\mathbb{E}[v_k]$ for each slot k . Note that this procedure breaks slot symmetry because $\boldsymbol{\alpha}^0$ assigns slots to default regions of the image.

Algorithm 1 Spatial Locality Prior. The algorithm takes image embedding features $Z \in \mathbb{R}^{N \times C}$; the number of slots, K ; the number of slot-update iterations, T_{slot} ; the number of spatial-update iterations, T_{spat} ; and the projection dimensionality, d . The learned model parameters are: the learned projections q, k, v each with dimensionality d , the alpha initialization $\alpha^0 \in \mathbb{R}^{K \times N}$; the **GRU** and the **MLP** layers; and a Gaussian mean and variance $\mu, \sigma \in \mathbb{R}^d$.

```

 $S \sim \mathcal{N}(\mu, \sigma)$ 
 $Z = \text{LayerNorm}(Z)$ 
 $\alpha = \alpha^0 / \|\alpha^0\|_2$ 
for  $i = 1 \dots T_{slot}$  do
   $S = \text{LayerNorm}(S)$ 
   $L = \frac{1}{\sqrt{d}} q(S) \cdot k(Z)^T$ 
  for  $j = 1 \dots T_{spat}$  do
    if  $j = T_{spat} - 1$  then
       $\alpha = \text{StopGradient}(\alpha) + \alpha^0 - \text{StopGradient}(\alpha^0)$ 
    end if
     $A = \text{Softmax}(L + \alpha, \text{axis} = \text{"slots"})$ 
     $m, v = \text{ComputeDistribution}(Z, A)$ 
     $l = \text{GetLoss}(\alpha, m, v)$ 
     $\alpha = \alpha - \alpha_{lr} \cdot \frac{\partial l}{\partial \alpha}$ 
  end for
   $A = \text{Softmax}(L + \alpha, \text{axis} = \text{"slots"})$ 
   $A = A / \text{sum}(A, \text{axis} = \text{"embeddings"})$ 
   $U = A \cdot v(Z)$ 
  for  $n = 1 \dots N$  in parallel do
     $S_n = \text{GRU}(S_n, U_n)$ 
     $S_n += \text{MLP}(\text{LayerNorm}(S_n))$ 
  end for
end for
return  $S$ 

```

▷ Compute Equation 1
 ▷ Compute Equations 2 and 3

4 Experiments

In this section, we evaluate the benefit of incorporating the spatial-locality prior into Slot Attention, as well as into two recent object-centric methods that build upon Slot Attention to achieve state-of-the-art performance, BO-QSA [Jia et al., 2023] and DINOSAUR [Seitzer et al., 2023]. We find that for all three models, across eight diverse datasets, the spatial-locality prior boosts performance. We refer to the base models (Slot Attention, BO-QSA, and DINOSAUR) augmented with the spatial locality prior (hereafter, *SLP*) by adding the modifier ‘+SLP’ to the name. All comparisons we report use a given base model with and without SLP for highly controlled experimentation.

Here we include details about our datasets, architectural decisions, and evaluation methods; but hyperparameters and other simulation details are presented in the Supplementary Materials. All experiments were run on a single 50GB Quatro RTX 8000 GPU.

4.1 Object Discovery in Synthetic Images

For synthetic datasets, we focus on the task of Object Discovery [Burgess et al., 2019], which is to produce a set of masks that cover each of the objects that appear in the image. We first isolate the effect of SLP through experimenting with vanilla Slot Attention [Locatello et al., 2020] on CLEVR6 [Johnson et al., 2016], ObjectsRoom [Kabra et al., 2019], MultidSprites [Burgess et al., 2019], ShapeStacks [Groth et al., 2018], and ClevrTex [Karazija et al., 2021]. To show that SLP works for other variants of Slot Attention, we examine BO-QSA [Jia et al., 2023] on ShapeStacks, ObjectsRoom, and ClevrTex datasets. We primarily focus on Foreground-ARI (FG-ARI) [Hubert and Arabie, 1985] as our dependent measure of performance. We then show results with DINOSAUR [Seitzer et al., 2023] on the MoVi-C and MoVi-E datasets [Greff et al., 2022], where we evaluate using FG-ARI and mean-best-overlap (mBO) [Pont-Tuset et al., 2015].

Table 1: Foreground ARI (%) Segmentation Accuracy
(mean \pm 1 SEM across 3 replications of each simulation)

(a) Results for Vanilla Slot Attention augmented with SLP

Method	ObjectsRoom	MultidSprites	ShapeStacks	ClevrTex
MONet [Burgess et al., 2019]	0.54 \pm 0.05	0.89 \pm 0.05	0.70 \pm 0.11	0.19 \pm 0.05
GENESIS-V2 [Engelcke et al., 2021]	0.86 \pm 0.05	0.52 \pm 0.15	0.81 \pm 0.05	0.31 \pm 0.20
Slot Attention [Locatello et al., 2020]	0.86 \pm 0.14	0.91 \pm 0.10	0.80 \pm 0.08	0.62 \pm 0.08
Slot Attention + SLP	0.87 \pm 0.05	0.94 \pm 0.05	0.83 \pm 0.05	0.71 \pm 0.05

(b) Varying hyperparameters (number of slot-update iterations and spatial-update iterations) for ClevrTex

Method	3 slot iterations	5 slot iterations	10 slot iterations
Slot Attention [Locatello et al., 2020]	0.45 \pm 0.23	0.35 \pm 0.20	0.34 \pm 0.16
Slot Attention + SLP (1 spatial iteration)	0.54 \pm 0.05	0.61 \pm 0.05	0.60 \pm 0.14
Slot Attention + SLP (5 spatial iterations)	0.64 \pm 0.10	0.60 \pm 0.08	0.63 \pm 0.11
Slot Attention + SLP (10 spatial iterations)	0.65 \pm 0.08	0.63 \pm 0.08	0.62 \pm 0.05

Table 2: FG-ARI (%) Accuracy
(mean \pm 1 SEM across 3 runs)
Varying number of slots for ClevrTex

Model	7 Slots	11 Slots
Slot Attention	0.45 \pm 0.23	0.62 \pm 0.08
Slot Attention + SLP	0.65 \pm 0.08	0.71 \pm 0.05

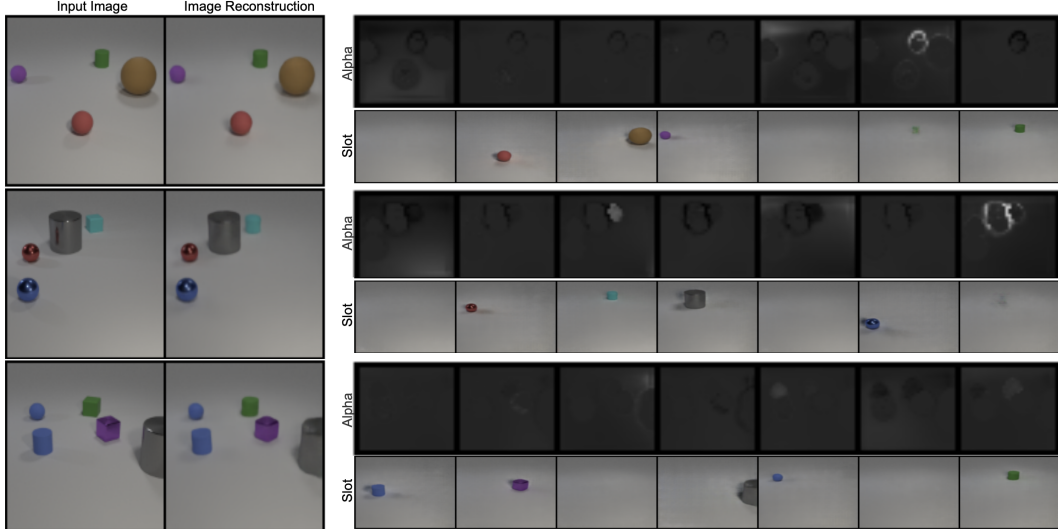
4.1.1 Vanilla Slot Attention

Methodology. In order to isolate the effect of SLP, we setup Slot Attention as described in Locatello et al. [2020], with a Mixture Decoder from Watters et al. [2019] and a 4-layer CNN encoder, on the object-discovery task. SLP is integrated into Slot Attention as described in Algorithm 1. Slots are initialized with a learned Gaussian mean and variance.

Results. Table 1a presents results for object discovery on synthetic datasets. Slot Attention + SLP yields improvements on MultidSprites, ShapeStacks, and, most notably, on ClevrTex. We obtain an almost 10% improvement on ClevrTex; given challenging views with diverse textures and complicated lighting effects, Slot Attention itself is not able to effectively segment the objects. SLP does not completely solve the task, but it is a significant step forward. Further, in Table 2, we show that SLP allows an underparametrized Slot Attention with 7 slots to match the 11 slot baseline. Additionally, the improvement on the 7 slot experiment is robust as a two-tailed t-test yielded $t(3) = 3.61, p = .02$.

Another limitation of vanilla Slot Attention is its fragility as the number of slot-update iterations across training and evaluation phase. In Table 1b, we show that SLP effectively solves this problem. In this Table, we manipulate both the number of slot-update iterations (T_{slot}) and the number of spatial-update iterations (T_{spat})—the columns and rows of the table, respectively. As the number of slot-update iterations increases, performance of Slot Attention drops but Slot Attention + SLP is not systematically affected. The Table also indicates that a single SLP iteration—minimal additional computation—provides a sufficient bias to improve FG-ARI.

The first and second columns of Figure 1a show three sample Clevr6 images and their reconstruction, respectively. To the right of each image pair is the α_k spatial-attention biases for each of the $k \in \{1 \dots 7\}$ slots (the dark images), and the the post-competition masked slot representations for each slot (color images). Note that the spatial-attention biases do not reflect the final selection, but rather the fact that SLP is encouraging slots to claim patches near already claimed patches. For some objects, especially in cases where the object seems to be distant, the spatial bias seems important, but not for all objects in these simple images.



(a) Clevr6 examples: Visualizations for Image Reconstructions, Slot Extractions, and Alphas.



(b) Visualization of meta-learned α^0 on Clevr6

Figure 1: Results from Slot Attention + SLP

Figure 1b visualizes the meta-learned initial spatial bias distribution, α^0 , for the 7 slots. The initialization essentially carves up the image, ignoring regions of the image that never contain objects. Note that these initial biases do not determine the final slot assignments, as one can see by inspection of the spatial distribution of objects claimed by a given slot in Figure 1a.

Figure 2 presents ClevrTex examples comparing Slot Attention and Slot Attention (SA) + SLP via image reconstructions and slot extractions. SA + SLP’s image reconstruction is far more accurate as compared to that of Slot Attention, with the clearest difference being the quality of the background scene and the overall image sharpness. This can be explained by the observation that *empty* slots of SA + SLP do a much better job of representing the background pattern. We also note that the slot decompositions are effectively localized with SA + SLP, even though the precise boundaries of the object are not sharp.

4.1.2 BO-QSA

Methodology. Here, the setup is identical to that in Section 4.1.1, the only difference being that the slots are set to learnable queries which are themselves learned through gradient updates via the straight-through estimator [Bengio et al., 2013].

Results. Table 3 presents FG-ARI scores for BO-QSA. Consistent with our previous results (4.1.1), we observe the largest improvements on ClevrTex, while also observing statistically reliable improvements on ShapeStacks and ObjectsRoom.

4.1.3 DINOSAUR

Methodology. We closely follow the setup of DINOSAUR [Seitzer et al., 2023], using a frozen pre-trained ViT encoder [Kolesnikov et al., 2021], Slot Attention with 11 slots for MoVi-C and 24 slots for MoVi-E, a Transformer Decoder similar to SLATE [Singh et al., 2022a] and feature reconstruction loss as the primary learning signal instead of image reconstruction loss.

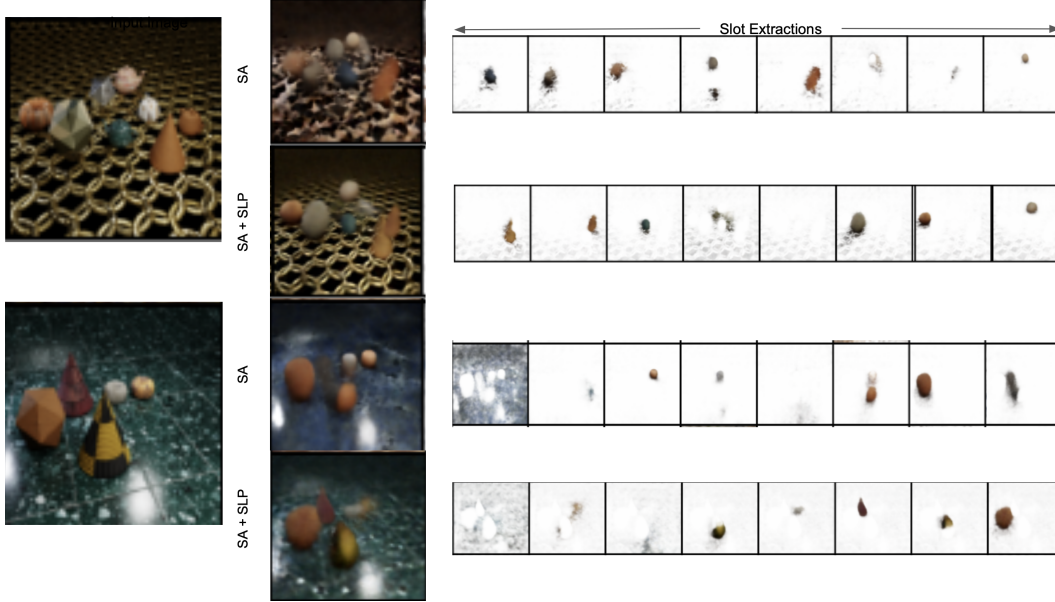


Figure 2: ClevrTex examples: Visualizing Image Reconstructions and Slot Extractions for Slot Attention (SA) and Slot Attention + SLP (SA + SLP)

Table 3: Foreground ARI (%) Segmentation Accuracy
(mean \pm 1 SEM across 3 replications of each simulation)
BO-QSA [Jia et al., 2023] augmented with SLP

Method	ShapeStacks	ObjectsRoom	ClevrTex
MONet [Burgess et al., 2019]	0.70 \pm 0.11	0.54 \pm 0.05	0.19 \pm 0.05
GENESIS-V2 [Engelcke et al., 2021]	0.81 \pm 0.05	0.86 \pm 0.05	0.31 \pm 0.20
SLATE [Singh et al., 2022a]	0.65 \pm 0.10	0.57 \pm 0.10	0.73 \pm 0.05
I-SA [Chang et al., 2022]	0.90 \pm 0.08	0.85 \pm 0.05	0.78 \pm 0.10
BO-QSA [Jia et al., 2023]	0.93 \pm 0.05	0.87 \pm 0.05	0.80 \pm 0.08
BO-QSA + SLP	0.95 \pm 0.08	0.93 \pm 0.05	0.87 \pm 0.05

Results. Table 4 compares measures of object discovery for MoVi-C and MoVi-E datasets on DINOSAUR and our augmented variant with SLP. On both data sets and two performance measures—FG-ARI and mBO—DINOSAUR + SLP reliably outperforms DINOSAUR.

4.2 Object Discovery in Real-World Images

For real-world data, following Jia et al. [2023] we use two tasks to evaluate BO-QSA + SLP: unsupervised foreground extraction and unsupervised multi-object segmentation. For unsupervised foreground extraction, we experiment on the CUB [Wah et al., 2011], Stanford Dogs [Khosla et al., 2012], and Stanford Cars [Krause et al., 2013] datasets and evaluate using Intersection-over-Union

Table 4: FG-ARI and mBO measures of object discovery
on MoVi-C and MoVi-E with DINOSAUR [Seitzer et al., 2023] (mean \pm 1 SEM across 3 runs)

Method	MoVi-C		MoVi-E	
	FG-ARI	mBO	FG-ARI	mBO
DINOSAUR (ViT-B/8)	68.9 \pm 0.3	38.0 \pm 0.2	65.1 \pm 0.6	33.5 \pm 0.1
DINOSAUR + SLP	72.8 \pm 0.6	41.5 \pm 0.3	70.4 \pm 0.4	35.9 \pm 0.2

Table 5: Real-World Image Experiments

(a) Unsupervised foreground extraction performance on BO-QSA [Jia et al., 2023] with and without SLP. Results from earlier baseline models are based on the *best* replication, whereas the our results are *mean* \pm 1 SEM performance across three replications per simulation.

Method	CUB		Stanford Dogs		Stanford Cars	
	IoU	Dice	IoU	Dice	IoU	Dice
ReDO [Chen et al., 2019]	0.46	0.60	0.55	0.70	0.52	0.68
IODINE [Greff et al., 2019b]	0.30	0.44	0.54	0.67	0.51	0.67
OneGAN [Benny and Wolf, 2019]	0.55	0.69	0.71	0.81	0.71	0.82
SLATE [Singh et al., 2022a]	0.36	0.51	0.62	0.76	0.75	0.85
I-SA [Chang et al., 2022]	0.63	0.72	0.80	0.89	0.85	0.92
BO-QSA [Jia et al., 2023]	0.61 \pm 0.12	0.74 \pm 0.12	0.78 \pm 0.12	0.68 \pm 0.04	0.76 \pm 0.05	0.86 \pm 0.05
BO-QSA + SLP	0.68 \pm 0.02	0.80 \pm 0.02	0.78 \pm 0.12	0.87 \pm 0.12	0.82 \pm 0.08	0.91 \pm 0.05

(b) Unsupervised multi-object segmentation using BO-QSA with and without SLP, following Yang and Yang [2022] (mean \pm 1 SEM across 3 replications of each simulation)

Method	COCO				ScanNet			
	AP@05	Precision	Recall	PQ	AP@05	Precision	Recall	PQ
BO-QSA	0.093 \pm 0.152	0.169 \pm 0.194	0.208 \pm 0.210	0.114 \pm 0.159	0.234 \pm 0.057	0.339 \pm 0.054	0.387 \pm 0.060	0.234 \pm 0.051
BO-QSA + SLP	0.126 \pm 0.115	0.206 \pm 0.129	0.251 \pm 0.142	0.139 \pm 0.100	0.261 \pm 0.060	0.349 \pm 0.048	0.399 \pm 0.051	0.242 \pm 0.040

(IoU) and Dice evaluation metrics. For unsupervised multi-object segmentation, we experiment on COCO [Lin et al., 2014] and ScanNet [Dai et al., 2017] datasets and evaluate using the metrics followed in Yang and Yang [2022]

Methodology. As our base model, we use BO-QSA [Jia et al., 2023] with the SLATE encoder-decoder setup [Singh et al., 2022a], which consists of a 4-layer CNN encoder and a Transformer decoder in a dVAE setup. The slots are initialized as learned embeddings and the initializations are optimized directly as in Jia et al. [2023]. During evaluation, we select predicted foreground as the one with the maximum intersection between slot’s mask prediction and ground-truth foreground mask.

Results. Table 5a presents results for unsupervised foreground extraction and Table 5b presents results for unsupervised multi-object segmentation. On all data sets and on both tasks, SLP consistently improves the performance of BO-QSA, the most significant improvement being on the Dice metric for the Stanford Dogs dataset. It appears that I-SA [Chang et al., 2022] marginally outperforms

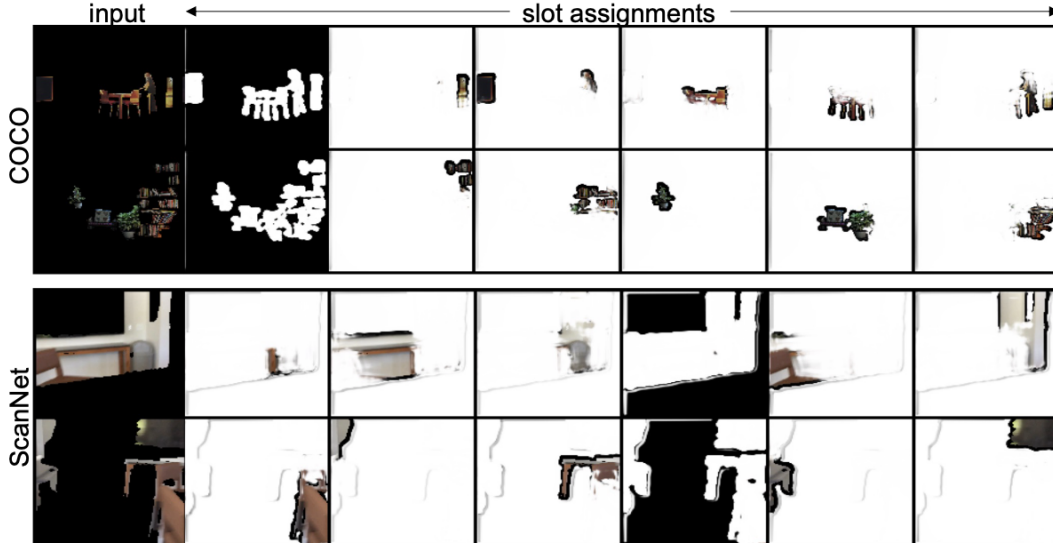


Figure 3: Slot assignments for BO-QSA + SLP on COCO and ScanNet.

Table 6: FG-ARI (%) and Mean-Squared Error (MSE)
BO-QSA Jia et al. [2023] with and without SLP
(mean \pm 1 SEM across 3 experiment trials)

Method	ClevrTex-OOD	
	FG-ARI	MSE
MONet [Burgess et al., 2019]	0.37 \pm 0.05	409 \pm 0.5
GENESIS-V2 [Engelcke et al., 2021]	0.29 \pm 0.19	539 \pm 7.0
Slot-Attention [Locatello et al., 2020]	0.58 \pm 0.05	487 \pm 2.3
I-SA [Chang et al., 2022]	0.83 \pm 0.05	241 \pm 1.1
BO-QSA [Jia et al., 2023]	0.86 \pm 0.05	265 \pm 2.9
BO-QSA + SLP	0.88 \pm 0.05	243 \pm 1.6

BO-QSA + SLP on Stanford Dogs and Stanford Cars. *However*, the baselines reported in Table 5a—including I-SA results—are the best performing replication of multiple runs, whereas we report mean performance across three replications for BO-QSA and BO-QSA + SLP. Figure 3 presents visualizations of slot assignments for several COCO images (first and second rows) and ScanNet images (third and fourth rows).

4.3 Out-of-Distribution Generalization

One potential weakness of our model is the explicit learning of α^0 based on training-set-wide statistics of the likely spatial locations of objects. This initialization may result in poor OOD generalization. However, we observe that this issue does not adversely affect our model. As suggested by Figure 1b, learning α^0 does help break symmetry: the learned α disperses the slot means across the scene while maintaining a high slot variance. As a result, the attention distribution forces the slots to model different objects in the scene. However, since the learned initialization is normalized before further optimization, the effects of an excessively large α^0 initialization should be effectively nullified.

As evidence in support of our conjecture, we tested Slot Attention with SLP and initialized slots as learned embeddings as in Section 4.1.2. We evaluate object discovery on the ClevrTex-OOD split variants and present results in Table 6. Empirically, as we see improvements both in FG-ARI and in MSE Reconstruction loss, we are able to prove that learning dataset wide statistics merely has the effect of learning an α^0 initialization that supports symmetry breaking between slots.

5 Discussion

In this paper, we proposed a spatial-locality prior that is consistent with both human visual attention and statistics of objects in natural images. Incorporating this prior into unsupervised object-centric models biases slot decompositions of the visual scene when direct evidence for objects and their boundaries is weak. The result is improved models that are more robust to hyperparameter selection and that yield better object segmentations. We show consistent improvements with three object-centric architectures (Slot Attention, BO-QSA, and DINOSAUR), eight distinct data sets, and various performance measures that have been used in the literature, including FG-ARI, mBO, IoU, and Dice. In all cases, models incorporating SLP advance state-of-the-art performance.

Limitations and Future Work. A key limitation of the proposed method—as well as of any slot-based object-centric model, is the hard requirement to specify the maximum number of slots that the model can represent. Another limitation of SLP in particular is the increased computational complexity due to the bi-level optimization algorithm. Fortunately, we have found that a single spatial iteration, which is relatively efficient, yields significant benefits. In future we hope to extend the proposed method from static images to video streams. SLP should be even more fruitful for video streams where the spatial modulations, α , inferred for one frame should be a suitable initialization point for the next frame. We also hope to extend the method to include the depth dimension of spatial attention, allowing SLP to operate in depth and to thereby predict occlusions.

6 Acknowledgement

This research was enabled in part by compute resources provided by Mila (mila.quebec). We would like to thank Vedant Shah and Aniket Didolkar for reviewing early versions of the manuscript. We would also like to thank Mihir Prabhudesai and Katerina Fragkiadaki for useful discussions.

References

- Zhipeng Bao, Pavel Tokmakov, Allan Jabri, Yu-Xiong Wang, Adrien Gaidon, and Martial Hebert. Discorring object that can move. In *CVPR*, 2022.
- Zhipeng Bao, Pavel Tokmakov, Yu-Xiong Wang, Adrien Gaidon, and Martial Hebert. Object discovery from motion-guided tokens. In *CVPR*, 2023.
- Yoshua Bengio, Nicholas Léonard, and Aaron C. Courville. Estimating or propagating gradients through stochastic neurons for conditional computation. *ArXiv*, abs/1308.3432, 2013.
- Yaniv Benny and Lior Wolf. Onegan: Simultaneous unsupervised learning of conditional image generation, foreground segmentation, and fine-grained clustering. *ArXiv*, abs/1912.13471, 2019.
- Ondrej Biza, Sjoerd van Steenkiste, Mehdi S. M. Sajjadi, Gamaleldin F. Elsayed, Aravindh Mahendran, and Thomas Kipf. Invariant slot attention: Object discovery with slot-centric reference frames. *ArXiv*, abs/2302.04973, 2023.
- Christopher P. Burgess, Loic Matthey, Nicholas Watters, Rishabh Kabra, Irina Higgins, Matt Botvinick, and Alexander Lerchner. Monet: Unsupervised scene decomposition and representation, 2019.
- Ayush K Chakravarthy, Jacob Labe Russin, and Randall O’Reilly. Systematicity emerges in transformers when abstract grammatical roles guide attention. In *Proceedings of the 2022 Conference of the North American Chapter of the Association for Computational Linguistics: Human Language Technologies: Student Research Workshop*, pages 1–8, Hybrid: Seattle, Washington + Online, July 2022. Association for Computational Linguistics. doi: 10.18653/v1/2022.naacl-srw.1. URL <https://aclanthology.org/2022.naacl-srw.1>.
- Michael Chang, Thomas L. Griffiths, and Sergey Levine. Object representations as fixed points: Training iterative refinement algorithms with implicit differentiation. *ArXiv*, abs/2207.00787, 2022.
- Mickaël Chen, Thierry Artières, and Ludovic Denoyer. Unsupervised object segmentation by redrawing. In *Neural Information Processing Systems*, 2019.
- Eric Crawford and Joelle Pineau. Spatially invariant unsupervised object detection with convolutional neural networks. In *Proceedings of the Thirty-Third AAAI Conference on Artificial Intelligence and Thirty-First Innovative Applications of Artificial Intelligence Conference and Ninth AAAI Symposium on Educational Advances in Artificial Intelligence*, AAAI’19/IAAI’19/EAAI’19. AAAI Press, 2019. ISBN 978-1-57735-809-1. doi: 10.1609/aaai.v33i01.33013412. URL <https://doi.org/10.1609/aaai.v33i01.33013412>.
- Angela Dai, Angel X. Chang, Manolis Savva, Maciej Halber, Thomas Funkhouser, and Matthias Nießner. Scannet: Richly-annotated 3d reconstructions of indoor scenes. In *2017 IEEE Conference on Computer Vision and Pattern Recognition (CVPR)*, pages 2432–2443, 2017. doi: 10.1109/CVPR.2017.261.
- Andrea Dittadi, Samuele S Papa, Michele De Vita, Bernhard Schölkopf, Ole Winther, and Francesco Locatello. Generalization and robustness implications in object-centric learning. In Kamalika Chaudhuri, Stefanie Jegelka, Le Song, Csaba Szepesvari, Gang Niu, and Sivan Sabato, editors, *Proceedings of the 39th International Conference on Machine Learning*, volume 162 of *Proceedings of Machine Learning Research*, pages 5221–5285. PMLR, 17–23 Jul 2022. URL <https://proceedings.mlr.press/v162/dittadi22a.html>.
- J. Duncan. Selective attention and the organization of visual information. *Journal of Experimental Psychology: General*, 113:501–517, 1984.

- Cathrin Elich, Martin R. Oswald, Marc Pollefeys, and Joerg Stueckler. Weakly supervised learning of multi-object 3d scene decompositions using deep shape priors. *Comput. Vis. Image Underst.*, 220:103440, 2020.
- Gamaleldin F. Elsayed, Aravindh Mahendran, Sjoerd van Steenkiste, Klaus Greff, Michael C. Mozer, and Thomas Kipf. SAVi++: Towards end-to-end object-centric learning from real-world videos. In *Advances in Neural Information Processing Systems*, 2022.
- Martin Engelcke, Oiwi Parker Jones, and Ingmar Posner. Genesis-v2: Inferring unordered object representations without iterative refinement. In *Neural Information Processing Systems*, 2021.
- S. M. Ali Eslami, Nicolas Heess, Theophane Weber, Yuval Tassa, David Szepesvari, Koray Kavukcuoglu, and Geoffrey E. Hinton. Attend, infer, repeat: Fast scene understanding with generative models. In *Proceedings of the 30th International Conference on Neural Information Processing Systems, NIPS’16*, page 3233–3241, Red Hook, NY, USA, 2016. Curran Associates Inc. ISBN 9781510838819.
- Jerry A. Fodor and Zenon W. Pylyshyn. Connectionism and cognitive architecture: A critical analysis. *Cognition*, 28(1-2):3–71, March 1988. ISSN 00100277. doi: 10.1016/0010-0277(88)90031-5.
- A. Goyal, A. Lamb, J. Hoffmann, S. Sodhani, S. Levine, Y. Bengio, and B. Schölkopf. Recurrent independent mechanisms. In *9th International Conference on Learning Representations (ICLR)*, May 2021a. URL <https://openreview.net/pdf?id=mLcmd1EUxy->.
- Anirudh Goyal and Yoshua Bengio. Inductive biases for deep learning of higher-level cognition. *Proceedings of the Royal Society A*, 478(2266):20210068, 2022.
- Anirudh Goyal, Alex Lamb, Phanideep Gampa, Philippe Beaudoin, Sergey Levine, Charles Blundell, Yoshua Bengio, and Michael Mozer. Object files and schemata: Factorizing declarative and procedural knowledge in dynamical systems, 2020.
- Anirudh Goyal, Aniket Didolkar, Nan Rosemary Ke, Charles Blundell, Philippe Beaudoin, Nicolas Heess, Michael C Mozer, and Yoshua Bengio. Neural production systems. *Advances in Neural Information Processing Systems*, 34:25673–25687, 2021b.
- Anirudh Goyal, Aniket Didolkar, Alex Lamb, Kartikeya Badola, Nan Rosemary Ke, Nasim Rahaman, Jonathan Binas, Charles Blundell, Michael Mozer, and Yoshua Bengio. Coordination among neural modules through a shared global workspace. *arXiv preprint arXiv:2103.01197*, 2021c.
- Klaus Greff, Sjoerd van Steenkiste, and Jürgen Schmidhuber. Neural expectation maximization. In *Proceedings of the 31st International Conference on Neural Information Processing Systems, NIPS’17*, page 6694–6704, Red Hook, NY, USA, 2017. Curran Associates Inc. ISBN 9781510860964.
- Klaus Greff, Raphael Lopez Kaufman, Rishabh Kabra, Nicholas Watters, Christopher P. Burgess, Daniel Zoran, Loïc Matthey, Matthew M. Botvinick, and Alexander Lerchner. Multi-object representation learning with iterative variational inference. In *International Conference on Machine Learning*, 2019a.
- Klaus Greff, Raphaël Lopez Kaufman, Rishabh Kabra, Nick Watters, Chris Burgess, Daniel Zoran, Loïc Matthey, Matthew M. Botvinick, and Alexander Lerchner. Multi-object representation learning with iterative variational inference. In Kamalika Chaudhuri and Ruslan Salakhutdinov, editors, *Proceedings of the 36th International Conference on Machine Learning, ICML 2019, 9-15 June 2019, Long Beach, California, USA*, volume 97 of *Proceedings of Machine Learning Research*, pages 2424–2433. PMLR, 2019b. URL <http://proceedings.mlr.press/v97/greff19a.html>.
- Klaus Greff, Sjoerd van Steenkiste, and Jürgen Schmidhuber. On the binding problem in artificial neural networks. *ArXiv*, abs/2012.05208, 2020.
- Klaus Greff, Francois Belletti, Lucas Beyer, Carl Doersch, Yilun Du, Daniel Duckworth, David J. Fleet, Dan Gnanapragasam, Florian Golemo, Charles Herrmann, Thomas Kipf, Abhijit Kundu, Dmitry Lagun, Issam Laradji, Hsueh-Ti (Derek) Liu, Henning Meyer, Yishu Miao, Derek

- Nowrouzezahrai, Cengiz Oztireli, Etienne Pot, Noha Radwan, Daniel Rebain, Sara Sabour, Mehdi S. M. Sajjadi, Matan Sela, Vincent Sitzmann, Austin Stone, Deqing Sun, Suhani Vora, Ziyu Wang, Tianhao Wu, Kwang Moo Yi, Fangcheng Zhong, and Andrea Tagliasacchi. Kubric: A scalable dataset generator. In *Proceedings of the IEEE/CVF Conference on Computer Vision and Pattern Recognition (CVPR)*, pages 3749–3761, June 2022.
- Karol Gregor, Ivo Danihelka, Alex Graves, Danilo Rezende, and Daan Wierstra. Draw: A recurrent neural network for image generation. In Francis Bach and David Blei, editors, *Proceedings of the 32nd International Conference on Machine Learning*, volume 37 of *Proceedings of Machine Learning Research*, pages 1462–1471, Lille, France, 07–09 Jul 2015. PMLR. URL <https://proceedings.mlr.press/v37/gregor15.html>.
- Oliver Groth, Fabian B. Fuchs, Ingmar Posner, and Andrea Vedaldi. Shapestacks: Learning vision-based physical intuition for generalised object stacking. In Vittorio Ferrari, Martial Hebert, Cristian Sminchisescu, and Yair Weiss, editors, *Computer Vision - ECCV 2018 - 15th European Conference, Munich, Germany, September 8-14, 2018, Proceedings, Part I*, volume 11205 of *Lecture Notes in Computer Science*, pages 724–739. Springer, 2018. doi: 10.1007/978-3-030-01246-5_43. URL https://doi.org/10.1007/978-3-030-01246-5_43.
- Lawrence J. Hubert and Phipps Arabie. Comparing partitions. *Journal of Classification*, 2:193–218, 1985.
- Baoxiong Jia, Yu Liu, and Siyuan Huang. Improving object-centric learning with query optimization. *International Conference on Learning Representations (ICLR)*, 2023.
- Jindong Jiang, Sepehr Janghorbani, Gerard de Melo, and Sungjin Ahn. Scalor: Generative world models with scalable object representations. In *Proceedings of ICLR 2020*. OpenReview.net, 2020. URL <https://openreview.net/pdf?id=SJxrKgStDH>.
- Justin Johnson, Bharath Hariharan, Laurens van der Maaten, Li Fei-Fei, C. Lawrence Zitnick, and Ross B. Girshick. Clevr: A diagnostic dataset for compositional language and elementary visual reasoning. *2017 IEEE Conference on Computer Vision and Pattern Recognition (CVPR)*, pages 1988–1997, 2016.
- Rishabh Kabra, Chris Burgess, Loic Matthey, Raphael Lopez Kaufman, Klaus Greff, Malcolm Reynolds, and Alexander Lerchner. Multi-object datasets. <https://github.com/deepmind/multi-object-datasets/>, 2019.
- Laurynas Karazija, Iro Laina, and C. Rupprecht. Clevrtex: A texture-rich benchmark for unsupervised multi-object segmentation. *ArXiv*, abs/2111.10265, 2021.
- Nan Rosemary Ke, Aniket Didolkar, Sarthak Mittal, Anirudh Goyal, Guillaume Lajoie, Stefan Bauer, Danilo Rezende, Yoshua Bengio, Michael Mozer, and Christopher Pal. Systematic evaluation of causal discovery in visual model based reinforcement learning. *arXiv preprint arXiv:2107.00848*, 2021.
- Aditya Khosla, Nityananda Jayadevaprakash, Bangpeng Yao, and Li Fei-Fei. Novel dataset for fine-grained image categorization : Stanford dogs. 2012.
- Jinwoo Kim, Janghyuk Choi, Ho-Jin Choi, and Seonhoon Kim. Shepherding slots to objects: Towards stable and robust object-centric learning. *ArXiv*, abs/2303.17842, 2023.
- Thomas Kipf, Gamaleldin F. Elsayed, Aravindh Mahendran, Austin Stone, Sara Sabour, Georg Heigold, Rico Jonschkowski, Alexey Dosovitskiy, and Klaus Greff. Conditional Object-Centric Learning from Video. In *International Conference on Learning Representations (ICLR)*, 2022.
- Alexander Kolesnikov, Alexey Dosovitskiy, Dirk Weissenborn, Georg Heigold, Jakob Uszkoreit, Lucas Beyer, Matthias Minderer, Mostafa Dehghani, Neil Houlsby, Sylvain Gelly, Thomas Unterthiner, and Xiaohua Zhai. An image is worth 16x16 words: Transformers for image recognition at scale. 2021.
- Jonathan Krause, Michael Stark, Jia Deng, and Li Fei-Fei. 3d object representations for fine-grained categorization. *2013 IEEE International Conference on Computer Vision Workshops*, pages 554–561, 2013.

- D. LaBerge. Spatial extent of attention to letters and words. *Journal of Experimental Psychology: Human Perception and Performance*, 9:371–379, 1983.
- Tsung-Yi Lin, Michael Maire, Serge J. Belongie, Lubomir D. Bourdev, Ross B. Girshick, James Hays, Pietro Perona, Deva Ramanan, Piotr Dollár, and C. Lawrence Zitnick. Microsoft COCO: common objects in context. *CoRR*, abs/1405.0312, 2014. URL <http://arxiv.org/abs/1405.0312>.
- Zhixuan Lin, Yi-Fu Wu, Skand Vishwanath Peri, Weihao Sun, Gautam Singh, Fei Deng, Jindong Jiang, and Sungjin Ahn. Space: Unsupervised object-oriented scene representation via spatial attention and decomposition. *ArXiv*, abs/2001.02407, 2020.
- Francesco Locatello, Dirk Weissenborn, Thomas Unterthiner, Aravindh Mahendran, Georg Heigold, Jakob Uszkoreit, Alexey Dosovitskiy, and Thomas Kipf. Object-centric learning with slot attention, 2020.
- M. C. Mozer. A connectionist model of selective attention in visual perception. In V. L. Patel and G. J. Groen, editors, *Proceedings of the Tenth Annual Conference of the Cognitive Science Society*, pages 195–201, Hillsdale, NJ, 1988. Earlbaum Associates.
- Jordi Pont-Tuset, Pablo Arbeláez, Jonathan T. Barron, Ferran Marqués, and Jitendra Malik. Multiscale combinatorial grouping for image segmentation and object proposal generation. *IEEE Transactions on Pattern Analysis and Machine Intelligence*, 39:128–140, 2015.
- M. I. Posner. Orienting of attention. *Quarterly Journal of Experimental Psychology*, 32:3–25, 1980.
- B. Schölkopf, F. Locatello, S. Bauer, N. R. Ke, N. Kalchbrenner, A. Goyal, and Y. Bengio. Toward causal representation learning. *Proceedings of the IEEE*, 109(5):612–634, 2021. doi: 10.1109/JPROC.2021.3058954. URL <https://ieeexplore.ieee.org/stamp/stamp.jsp?arnumber=9363924>.
- Maximilian Seitzer, Max Horn, Andrii Zadaianchuk, Dominik Zietlow, Tianjun Xiao, Carl-Johann Simon-Gabriel, Tong He, Zheng Zhang, Bernhard Schölkopf, Thomas Brox, and Francesco Locatello. Bridging the gap to real-world object-centric learning. In *ICLR 2023*, 2023. URL <https://www.amazon.science/publications/bridging-the-gap-to-real-world-object-centric-learning>.
- Gautam Singh, Fei Deng, and Sungjin Ahn. Illiterate dall-e learns to compose. In *International Conference on Learning Representations*, 2022a. URL <https://openreview.net/forum?id=h00YV0We3oh>.
- Gautam Singh, Yi-Fu Wu, and Sungjin Ahn. Simple unsupervised object-centric learning for complex and naturalistic videos. In Alice H. Oh, Alekh Agarwal, Danielle Belgrave, and Kyunghyun Cho, editors, *Advances in Neural Information Processing Systems*, 2022b. URL <https://openreview.net/forum?id=eYfIM88MTUE>.
- Elizabeth S. Spelke and Katherine D. Kinzler. Core knowledge. *Developmental Science*, 10(1):89–96, 2007. doi: <https://doi.org/10.1111/j.1467-7687.2007.00569.x>. URL <https://onlinelibrary.wiley.com/doi/abs/10.1111/j.1467-7687.2007.00569.x>.
- Manuel Traub, Sebastian Otte, Tobias Menge, Matthias Karlbauer, Jannik Thümmel, and Martin V. Butz. Learning what and where: Disentangling location and identity tracking without supervision, 2023.
- Aäron van den Oord, Oriol Vinyals, and Koray Kavukcuoglu. Neural discrete representation learning. In *NIPS*, 2017.
- S. P. Vecera and M. J. Farah. Does visual attention select objects or locations? *Journal of Experimental Psychology: General*, 123:146–160, 1994.
- Catherine Wah, Steve Branson, Peter Welinder, Pietro Perona, and Serge J. Belongie. The caltech-ucsd birds-200-2011 dataset. 2011.

- Nicholas Watters, Loïc Matthey, Christopher P. Burgess, and Alexander Lerchner. Spatial broadcast decoder: A simple architecture for learning disentangled representations in vaes. *ArXiv*, abs/1901.07017, 2019.
- Marissa A. Weis, Kashyap Chitta, Yash Sharma, Wieland Brendel, Matthias Bethge, Andreas Geiger, and Alexander S. Ecker. Benchmarking unsupervised object representations for video sequences. *J. Mach. Learn. Res.*, 22(1), jan 2021. ISSN 1532-4435.
- Alfred North Whitehead. Symbolism: Its meaning and effect. *Humana Mente*, 3(12):527–530, 1928.
- Yafei Yang and Bo Yang. Promising or elusive? unsupervised object segmentation from real-world single images. *NeurIPS*, 2022.
- R. S. Zemel, M. Behrmann, M. C. Mozer, and D. Bavelier. Experience-dependent perceptual grouping and object-based attention. *Journal of Experimental Psychology: Human Perception and Performance*, 28:202–217, 2002.

Table 7: Spatial Locality Prior Configuration Sweep

α_{lr}	[1.0, 0.5, 0.1]
λ_{norm}	0.1
spatial iterations	[1, 5, 10, 20, 25]

7 SLP Configuration

In order to ensure robust experimentation, we adhere to the default hyperparameters¹ used in the previously reported results. We achieve this by augmenting various open-sourced and official implementations of each model, which serve as our baselines. The only exception we made was in determining the batch size, which was influenced by the hardware available to us.

Since each dataset and model exhibit different learning dynamics and scene complexities, we tune the hyperparameters of the SLP according to the sweep configuration outlined in Table 7. Through experimentation, we have found that setting α_{lr} to 1.0 consistently yields the best results. Consequently, we exclude the inferior results obtained with other values of α_{lr} from our analysis.

Generally, we observe that a larger number of spatial iterations is necessary to learn the appropriate spatial bias for scenes derived from more complex real-world datasets like COCO and ScanNet. Conversely, smaller values of spatial iterations tend to suffice for simpler and synthetic datasets such as ClevrTex. For example, as shown in Table 1b, setting $T_{spat} = 1$ brings about a significant performance improvement for 7-slot Slot Attention on ClevrTex.

Furthermore, we have discovered that annealing α_{lr} by a factor of $(T_{spat} - j) / T_{spat}$ enhances optimization dynamics. Our hypothesis is that initializing α_{lr} at 1.0 and subsequently annealing it results in a few aggressive steps towards the optimum, followed by several fine-tuning steps.

7.1 Vanilla Slot Attention Experiments

For the experiments conducted in Section 4.1.1, we utilized the open-source implementation provided by Dittadi et al. [2022]². In Table 8, an extension of Table 1b, we include higher values of spatial iterations. However, we observe minimal gains in performance when increasing the spatial iterations from 5 to 15. This leads us to hypothesize that the design of annealing α_{lr} starting from 1.0 encourages rapid convergence to a near-optimal α , and further increasing the number of spatial iterations does not yield significant performance improvements. Importantly, we did not observe any degradation in performance for any number of spatial iterations, indicating that SLP does not introduce additional gradient instability as observed when increasing the number of slot iterations in Slot Attention and its variants.

Table 8: Foreground ARI (%) Segmentation Accuracy
(mean \pm 1 SEM across 3 replications of each simulation)
Varying spatial iterations for 7-slot Slot Attention on ClevrTex

Slot Attention [Locatello et al., 2020]	0.47 \pm 0.22
Slot Attention + SLP (1 spatial iteration)	0.54 \pm 0.05
Slot Attention + SLP (5 spatial iterations)	0.64 \pm 0.10
Slot Attention + SLP (10 spatial iterations)	0.65 \pm 0.08
Slot Attention + SLP (15 spatial iterations)	0.66 \pm 0.05

7.2 BO-QSA experiments

For the experiments conducted in Sections 4.1.2 and 4.2, we built on the open-source implementation provided by Jia et al. [2023]³. In Tables 9 and 10, we extend Tables 3 and 6 respectively to include

¹For details on the default hyperparameters, please refer to the original papers.

²<https://github.com/addtt/object-centric-library>

³<https://github.com/YuLiu-LY/BO-QSA>

higher values of spatial iterations. Through these extensions, we were able to validate our hypothesis regarding the lack of improvement beyond a certain number of spatial iterations.

Specifically, in Table 3, we observe that increasing the number of spatial iterations to 5 does not result in a significant performance improvement on ClevrTex. However, as demonstrated in Table 8, setting SLP to 5 spatial iterations leads to a significant enhancement in performance. This suggests that the hyperparameter for spatial iterations is sensitive not only to dataset complexity but also to the learning dynamics of the model being used.

Table 9: Foreground ARI (%) Segmentation Accuracy
(mean \pm 1 SEM across 3 replications of each simulation)
BO-QSA [Jia et al., 2023] augmented with SLP
Varying spatial iterations

Method	ShapeStacks	ObjectsRoom	ClevrTex
BO-QSA [Jia et al., 2023]	0.93 \pm 0.05	0.87 \pm 0.05	0.80 \pm 0.08
BO-QSA + SLP (5 spatial iterations)	0.93 \pm 0.10	0.92 \pm 0.08	0.82 \pm 0.05
BO-QSA + SLP (10 spatial iterations)	0.95 \pm 0.08	0.93 \pm 0.05	0.87 \pm 0.05

Table 10: FG-ARI (%) and Mean-Squared Error (MSE)
BO-QSA Jia et al. [2023] with and without SLP
(mean \pm 1 SEM across 3 experiment trials)
Varying spatial iterations

Method	ClevrTex-OOD	
	FG-ARI	MSE
BO-QSA [Jia et al., 2023]	0.86 \pm 0.05	265 \pm 2.9
BO-QSA + SLP (10 spatial iterations)	0.88 \pm 0.05	243 \pm 1.6
BO-QSA + SLP (20 spatial iterations)	0.89 \pm 0.05	239 \pm 1.4
BO-QSA + SLP (25 spatial iterations)	0.89 \pm 0.05	242 \pm 0.8

7.3 DINOSAUR experiments

For the experiments conducted in Section 4.1.3, we built upon the open-source implementation provided by Seitzer et al. [2023]⁴. In these experiments, we were able to run higher values of spatial iterations, as demonstrated in Table 11. This was possible because DINOSAUR utilizes a frozen pre-trained ViT-B/8 encoder, resulting in a lower number of effective model parameters. Interestingly, we observed significant improvements for higher values of spatial iterations, which can be attributed to the fact that the DINOSAUR model does not apply any positional encoding to the encoded image representation. These results provide further evidence that SLP offers a stronger spatial bias compared to the positional encoding layer. They also suggest that existing methods which use positional encoding layers, need a stronger spatial bias which SLP provides.

Table 11: FG-ARI and mBO measures of object discovery
on MoVi-C and MoVi-E with DINOSAUR [Seitzer et al., 2023] (mean \pm 1 SEM across 3 runs).

Method	MoVi-C		MoVi-E	
	FG-ARI	mBO	FG-ARI	mBO
DINOSAUR (ViT-B/8)	68.9 \pm 0.3	38.0 \pm 0.2	65.1 \pm 0.6	33.5 \pm 0.1
DINOSAUR + SLP (10 spatial iterations)	70.1 \pm 0.4	38.5 \pm 0.2	66.3 \pm 0.6	34.5 \pm 0.3
DINOSAUR + SLP (20 spatial iterations)	72.8 \pm 0.6	41.5 \pm 0.3	70.4 \pm 0.4	35.9 \pm 0.2
DINOSAUR + SLP (50 spatial iterations)	74.6	42.6	73.1	36.7

⁴<https://github.com/amazon-science/object-centric-learning-framework>